nature physics

LETTERS

PUBLISHED ONLINE: 14 SEPTEMBER 2015 | DOI: 10.1038/NPHYS3459

Velocity tuning of friction with two trapped atoms

Dorian Gangloff[1†], Alexei Bylinskii[1†], Ian Counts[1], Wonho Jhe[2] and Vladan Vuletić[1*]

Our ability to control friction remains modest, as our understanding of the underlying microscopic processes is incomplete[1–3]. Atomic force experiments[4–14] have provided a wealth of results on the dependence of nanofriction on structure[5,6], velocity[7–10] and temperature[11–13], but limitations in the dynamic range, time resolution, and control at the single-atom level have hampered a description from first principles[3]. Here, using an ion-crystal system with single-atom, single-substrate-site spatial and single-slip temporal resolution[15,16], we measure the friction force over nearly five orders of magnitude in velocity, and contiguously observe four distinct regimes, while controlling temperature and dissipation. We elucidate the interplay between thermal and structural lubricity for two coupled atoms, and provide a simple explanation in terms of the Peierls–Nabarro potential[17]. This extensive control at the atomic scale enables fundamental studies of the interaction of many-atom surfaces, possibly into the quantum regime.

In the simplest scenario for stick–slip friction, a single atom at an object–substrate interface experiences a force resisting its motion due to a periodic potential created by the substrate[2] (Fig. 1a). A finite external force is then required to cause the atom to slip from one potential well to the next across an energy barrier U_B. Interestingly, in the case of more than one atom forming the contact interface, friction can be greatly reduced by a structural mismatch of the object and substrate, an effect coined superlubricity[5,6,15,18], and observed in friction force microscopy[5,6], colloidal monolayers[19], and recently in our friction simulator[15]. Thermally activated transitions between neighbouring potential wells at temperatures $T \sim U_B$ can also reduce the friction force significantly, making it velocity-dependent[7–10,13,20–24]. Separate observations have spanned from the high-temperature regime of thermolubricity[21] to the low-temperature regime of strong stick–slip[8]. In the present work, as a function of velocity, we observe the continuous transition between four regimes: thermal drift[21], where friction is small and (nearly) velocity-independent; thermal activation[7,8,10,21,24], where friction increases logarithmically with velocity; the friction plateau[8,9], where friction is large and nearly velocity-independent; and velocity weakening[20], where friction decreases with velocity because the damping is not fast enough to remove the energy released in a slip. For a two-atom contact, we observe that the measured friction force is substantially reduced by the interaction between the atoms when they are arranged so as to cancel the forces from the substrate. In our previous work[15], we had observed this effect for multiple atoms as a continuous transition from stick–slip to superlubricity when varying the arrangement of the atoms, while driving at a fixed large velocity where thermal effects are minor. In the present work, we link this structural lubricity to a reduced barrier $\widetilde{U}_B < U_B$ in the Peierls–Nabarro potential[17,25,26], and distinguish structurally induced thermolubricity ($T \sim \widetilde{U}_B$) from structural lubricity ($T \ll \widetilde{U}_B$) by observing the full velocity dependence.

Our implementation[15,16,27] of a friction interface, which simulates solid-state nanofriction[26,28,29] with an atomically sharp tip[4], consists of one or two electrically trapped atomic ions pulled against the sinusoidal potential (Fig. 1a,b) of a standing wave of light (optical lattice)[16,30,31]. We observe each ion's trajectory with resolution finer than the lattice period by means of the ion's position-dependent fluorescence[15]. Each time the ion slips into the next well, its fluorescence reaches a maximum and decreases as the ion is laser-cooled into the new potential minimum (Fig. 1c,d). Hysteresis in the timing of the slip as the electrostatic parabolic trapping potential is pulled back and forth reveals the maximum static friction force exerted by the lattice on the ion (Fig. 1d). At finite ion temperature T, the observed hysteresis and corresponding friction force are reduced (Fig. 1c,d).

At zero temperature[2,3,22], the dynamical behaviour is determined by the ratio of the lattice confinement frequency $\omega_l \propto \sqrt{U_l}$ to the electrostatic confinement frequency $\omega_0 \propto \sqrt{K}$, where U_l is the depth of the lattice potential, and K is the spring constant of the electrostatic trap (Fig. 1a). The corresponding dimensionless corrugation parameter $\eta = \omega_l^2/\omega_0^2$ determines the number of minima in the overall potential energy landscape. For $\eta \leq 1$, there is no stick–slip friction as only a single minimum is translated with the applied force. In our regime of interest, $1 < \eta < 4.6$, there are at most two local minima in the overall potential at any time, separated by a maximum energy barrier $U_B/U_l \simeq (\eta-1)^2/\eta^2$. At finite temperature, the ion can also slip owing to thermal activation before the barrier height is reduced to zero by the applied force (Fig. 1c), leading to a reduced hysteresis and friction (thermolubricity) that depend on the transport velocity v.

We observe, for the first time in a single experiment, four contiguous regimes of friction with distinct velocity dependences (Fig. 2a). These regimes can be organized by the hierarchy of three timescales, namely the thermal hopping time between lattice wells τ_{th}, the transport time for the external trap to move by one lattice well a/v, and the ion recooling time τ_c. When $\tau_{th} \ll a/v$, thermal hopping dominates, and the ion remains in thermal equilibrium, following the slowly moving ion trap—a regime called thermal drift, where the friction force due to stick–slip (almost) vanishes[21]. In the thermal activation regime $\tau_{th} \sim a/v$, the stick–slip process is only partially suppressed by thermal fluctuations and contributes to an average friction force, which grows logarithmically with velocity[7]. For even larger velocities $\tau_{th} \gg a/v \gg \tau_c$, thermal hopping across lattice wells is negligible on the transport timescale a/v. This is the friction plateau regime, where the friction force reaches its maximum value[8]. We also observe a fourth regime of friction, sometimes called velocity weakening[20], where the friction force decreases logarithmically with velocity[13]. In our system, this regime arises because the ion does not have sufficient

[1]Department of Physics, MIT-Harvard Center for Ultracold Atoms, and Research Laboratory of Electronics, Massachusetts Institute of Technology, Cambridge, Massachusetts 02139, USA. [2]Department of Physics and Astronomy, Seoul National University, Seoul 151-747, Korea. †These authors contributed equally to this work. *e-mail: vuletic@mit.edu

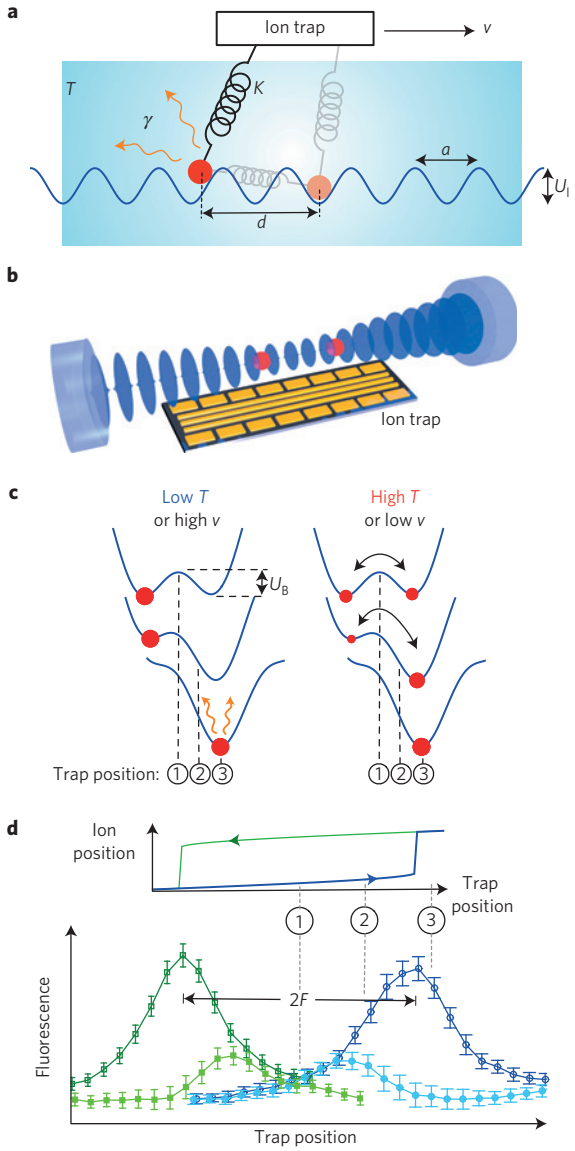

Figure 1 | Friction interface with trapped atomic ions in an optical lattice. **a**,**b**, Model of the friction interface; one Yb^+ ion of mass $m = 2.9 \times 10^{-25}$ kg (or two coupled ions separated by a distance $d \approx 5\,\mu$m) is confined in a Paul trap[27] with a spring constant $K = m\omega_0^2$ ($\omega_0/2\pi = 363$ kHz), whose equilibrium point is translated at a constant velocity v by applying a time-varying electric field. An optical standing wave, detuned by ~12 GHz from the atomic $^2S_{1/2} \rightarrow {}^2P_{1/2}$ transition, creates a sinusoidal potential of periodicity $a = 185$ nm and depth $U_l/h \approx 20$ MHz along the radiofrequency nodal line of the Paul trap[16]. The ion is kept at a temperature $T \approx 40\,\mu$K by means of continuous laser cooling with a dissipation rate constant $\gamma = \tau_c^{-1} \approx 10^4$ s^{-1}. **c**,**d**, Temperature dependence of stick–slip friction. At low temperature or high velocity, the ion (red solid circle) sticks in its initial well, corresponding to a rise in its scattered fluorescence (1–2, dark blue open circles) until it slips to the next well, and the added energy is dissipated through laser cooling (3, dark blue open circles). The ion fluorescence is highest when the slip occurs. At high temperature or low velocity, the ion thermalizes over the energy barrier (1–2), and so smoothly transitions to the next well without frictional dissipation (3). If the trap translation direction is reversed, maximum hysteresis is observed in the low-temperature or high-velocity regime (dark open symbols). A reduced hysteresis is present for an intermediate temperature or velocity regime (light filled symbols). The friction force F is measured by means of the separation $2F$ between the slips in the hysteresis loop. Error bars are statistical and represent one standard deviation.

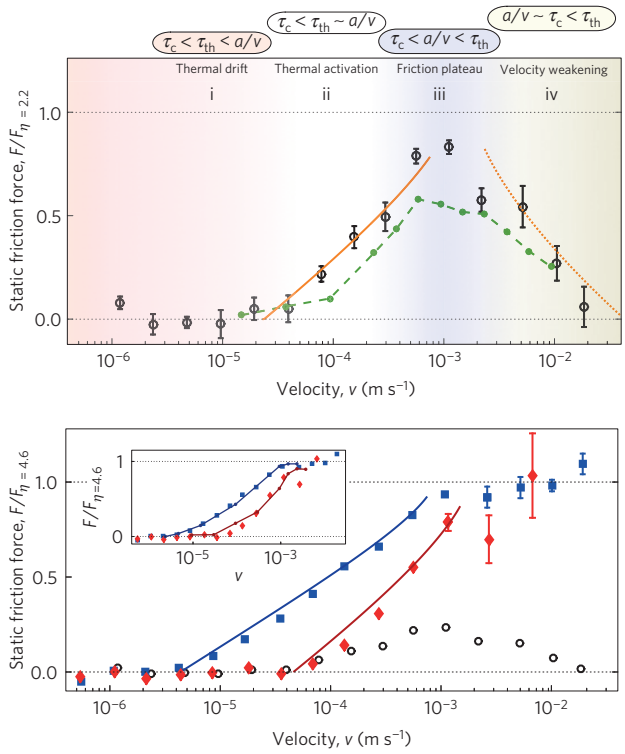

Figure 2 | Velocity dependence of stick–slip friction for one atom. The transport time a/v should be compared to two timescales: the thermal hopping time between two lattice wells, given by $\tau_{th} = \tau_0 \exp(U_B/k_B T)$ for a maximum barrier height U_B (where k_B is the Boltzmann constant and $\tau_0(\tau_c, \omega_0, \omega_l)$ is the hopping attempt time[23,24]); and the recooling time after a slip τ_c. **a**, Here $\tau_{th} \approx 10$ ms and $\tau_c \approx 100\,\mu$s. Four regimes of friction are observed. The friction force is normalized by its zero-temperature maximum value for $\eta = 2.2$, $F_{\eta=2.2} \approx 0.36\pi U_l/a$. Here $U_l/h = 9.5$ MHz and $k_B T/U_l = 0.15(4)$. The solid orange line shows the expected result $F/F_{\eta=2.2} = 1 - ((3/2\sqrt{2})(k_B T/U_l)\log(v_{th}/v))^{2/3}$, where $v_{th} \sim 1$ mm s^{-1}, from an analytical model in the thermal activation regime[3,23,24]. Similarly in the velocity weakening regime, we model the friction as $F/F_{\eta=2.2} = 1 - ((3/2\sqrt{2})(k_B T/U_l)\log(v/v_c))^{2/3}$ (orange dotted line), where $k_B T/U_l = 0.3$ and $v_c = a/\tau_c \sim 2$ mm s^{-1} (Supplementary Information). The Langevin simulation (dashed green line) is in good agreement with the data over all four velocity regimes for parameters $\eta = 2.2$, $k_B T/U_l = 0.15$, $\tau_c = 100\,\mu$s. **b**, At a larger lattice depth $U_l/h = 20$ MHz, where $\eta = 4.6$, increasing the temperature from $k_B T/U_l = 0.04(1)$ (blue squares) to $k_B T/U_l = 0.17(1)$ (red diamonds) reduces the friction in the thermal activation region 10^{-5} m s$^{-1} \lesssim v \lesssim 10^{-3}$ m s^{-1} while leaving the friction plateau in the region 10^{-3} m s$^{-1} \lesssim v \lesssim 10^{-2}$ m s^{-1} almost unaffected. Here, $\tau_c \approx 50\,\mu$s. The friction force is normalized by its zero-temperature maximum value for $\eta = 4.6$, $F_{\eta=4.6} \approx 0.61\pi U_l/a$. Solid lines show the expected results from the analytical thermal activation model. Data from **a**, normalized to $F_{\eta=4.6}$ is shown as open black circles. Langevin simulations (inset, solid lines) are in good agreement with the data for parameters $\eta = 4.6$, $k_B T/U_l = 0.05$ (blue), $k_B T/U_l = 0.13$ (red), $\tau_c = 50\,\mu$s. Error bars are statistical and represent one standard deviation.

time to recool after the slip for $a/v \lesssim \tau_c$. This effectively increases the ion's kinetic energy before the next slip event and reduces the friction force (Fig. 2a). Having direct access to all system parameters through independent microscopic measurements, we also show a full-dynamics simulation[22,23], without any free parameters, that closely follows our data over all four regimes of friction. Figure 2a furthermore shows that, in the thermal activation and velocity weakening regimes, simple analytical models for the velocity-dependent friction developed previously[3,23,24] match our data quantitatively

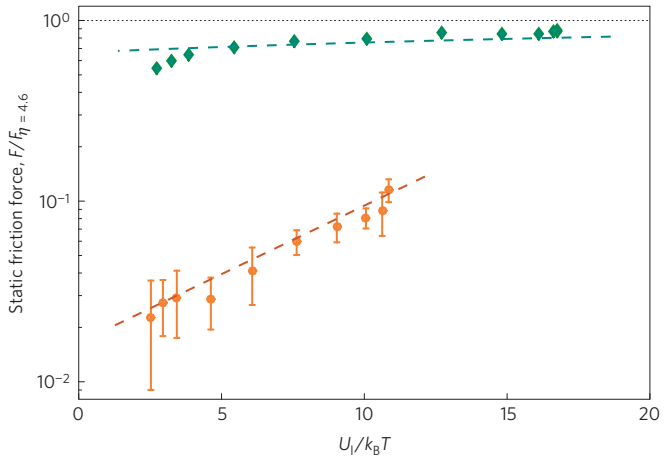

Figure 3 | Thermolubricity for a single atom. In the thermal drift regime $\tau_{th} \ll a/v$, the friction force is proportional to $\exp(U_l/k_BT)$, whereas it depends only weakly on temperature in the friction plateau regime[23] $\tau_{th} \gg a/v$. We vary temperature from $k_BT/U_l = 0.06$ to $k_BT/U_l = 0.4$, and show the friction force on a logarithmic scale against $1/T$. We fit data to the model $F/F_{\eta=4.6} = f\exp(cU_l/k_BT)$, where f is a free parameter, and c represents the fitted sensitivity to temperature and is close to unity in the thermal drift regime. For a high velocity ($v \approx 1\,mm\,s^{-1}$) corresponding to the friction plateau regime (green), friction is almost constant for $U_l/k_BT \geq 5$, and the fit to the model in this temperature range (dashed green line) gives $c = 0.016$—that is, a very weak temperature dependence. For a low velocity ($v \approx 40\,\mu m\,s^{-1}$) close to the regime of thermal drift (orange), the friction force is sensitive to temperature, and the fit to the model (red dashed line) gives $c = 0.17$. Experimental parameters are $\eta = 4.6$, $U_l/h = 20$ MHz and $\tau_c \approx 50\,\mu s$. Error bars are statistical and represent one standard deviation.

(Supplementary Information). The same good agreement between experimental data and theoretical models is attained when we change the barrier depth U_B or the temperature T (Fig. 2b).

The friction force is expected to be particularly sensitive to temperature when $\tau_{th} \lesssim a/v$, owing to exponential activation[21], and almost independent of it when $\tau_{th} \gg a/v$. In Fig. 3, we verify experimentally[11–13] that for low velocities ($\tau_{th} \leq a/v$) the friction force changes by an order of magnitude when we change the temperature by a factor of seven (Supplementary Information), whereas for high velocities ($\tau_{th} \gg a/v$) the force varies by less than a factor of two. This confirms that an effectively zero-temperature stick–slip regime[15] can be experimentally accessed at high transport velocity $v \gg a/\tau_{th}$.

To study the interplay between structural lubricity, arising from mismatch between the object and substrate corrugations, and thermolubricity, we place a second ion in the trap along the optical lattice direction (Fig. 1a,b). If the effective spring force arising from the Coulomb interaction between the ions were infinitely stiff, the friction force on the two-ion system could be made to vanish by placing the two ions at positions where they experience opposite lattice forces. It is the essence of structural lubricity that a substantial friction reduction persists even for finite ion–ion interaction that is comparable to the substrate corrugation. When the ions experience opposite lattice forces, it is energetically favourable for them to pass the energy barrier between wells one at a time, as illustrated by the two-dimensional energy landscapes of Fig. 4d,e. This results in a reduced barrier depth $\widetilde{U}_B < U_B$, and therefore a reduced friction force. Using the electrical trap, the spacing d between the ions can be tuned to be an exact multiple of a (that is, $d \bmod a = 0$), or to be mismatched (that is, $d \bmod a = a/2$). We have found in our previous work that mismatch greatly reduces the friction force[15], as has been also observed for graphite flakes on a graphite substrate under certain orientations[5].

Table 1 | Comparison of parameters in solid-state systems and in the present study.

	Solid state	Ion crystal
Lattice constant a (nm)	0.2–0.5 (refs 4,8)	185
Lattice depth U_l (eV)	0.1–2 (refs 8,13)	8×10^{-8}
Temperature T (K)	100–500 (ref. 11)	4×10^{-5}–4×10^{-4}
Tip/trap stiffness $K = m\omega_0^2$ (N m^{-1})	0.1–5 (refs 10,12)	1.5×10^{-12}
Velocity v (nm s^{-1})	1–10^6 (ref. 9)	500–2×10^7
Attempt frequency $f_0 = \tau_0^{-1}/2\pi$ (kHz)	2–1,000 (refs 9,21,24)	500
Damping rate $\gamma = \tau_c^{-1}$ (s^{-1})	10^5–10^6 (refs 23,24)	10^4, 2×10^4
Transport rate v/a (s^{-1})	10–10^7	2–10^5
Corrugation parameter $\eta \propto U_l/Ka^2$	1–8 (refs 6,21)	2.2, 4.6
Temperature parameter k_BT/U_l	0.02–0.5 (refs 11,12)	0.04–0.4

The friction reduction can be due to pure structural lubricity (stick–slip motion in a Peierls–Nabarro potential[17] with reduced energy barrier $\widetilde{U}_B \gg k_BT$) or to structurally induced thermolubricity ($\widetilde{U}_B \sim k_BT$), easily distinguished experimentally, as only the latter is velocity-dependent.

In the matched case, the two-ion system is expected to behave as a rigid object akin to a single particle, because only the centre-of-mass mode is affected by lattice forces. Figure 4a shows that the observed velocity dependence of friction in the matched case indeed agrees with the one-ion case. In the mismatched case, the lattice forces on the centre-of-mass mode cancel out, and we observe that, for the same temperature, friction is significantly reduced compared to the matched case (Fig. 4b), in good agreement with Langevin simulations. When comparing the friction in the mismatched case to the matched case, we find that there is no reduction in the thermal drift regime, and reduction by a factor of ~4.8 in the friction plateau regime (Fig. 4c). A calculation of the two-ion energy landscape (Fig. 4d,e) shows that in the matched case the barrier is identical to the one-ion case, whereas in the mismatched case it is approximately four times lower ($\widetilde{U}_B/U_B \simeq 3.7$). The additional ~20% friction reduction compared to $\widetilde{U}_B/U_B$ can be explained by structurally induced thermolubricity at fixed temperature due to the lower barrier depth $\widetilde{U}_B$ (Fig. 3). The high-velocity friction reduction plateau of Fig. 4c, where thermal hopping is negligible, then represents a direct observation of structurally induced lubricity or 'superlubricity'[5,6,15,18]. This interpretation is consistent with the observation that, in this regime, the ions pass the barrier one at a time (Fig. 4e inset), reminiscent of a kink defect being transported across the two-atom chain[17]. Thus, measuring the reduced friction force directly reveals the Peierls–Nabarro barrier[17] $\widetilde{U}_B$ for two atoms in a periodic potential.

To facilitate comparison of our ion-crystal system with typical solid-state systems, Table 1 summarizes the important physical parameters at play. Although parameters such as the lattice spacing a, the lattice depth U_l, the spring constant K, and the temperature T differ by several orders of magnitude, the important dimensionless parameters[2,3,21] that govern the frictional behaviour take on the same range of values in the two systems. In the future, the ion-crystal system could be used to study the more complex behaviours found in the multi-slip friction regime[14], and many-body phenomena arising from the strong particle interactions in the corrugated potential, such as the Aubry transition[2,17,26,29]. Furthermore, cooling to the vibrational ground state may provide access to a regime of quantum friction dominated by quantum tunnelling.

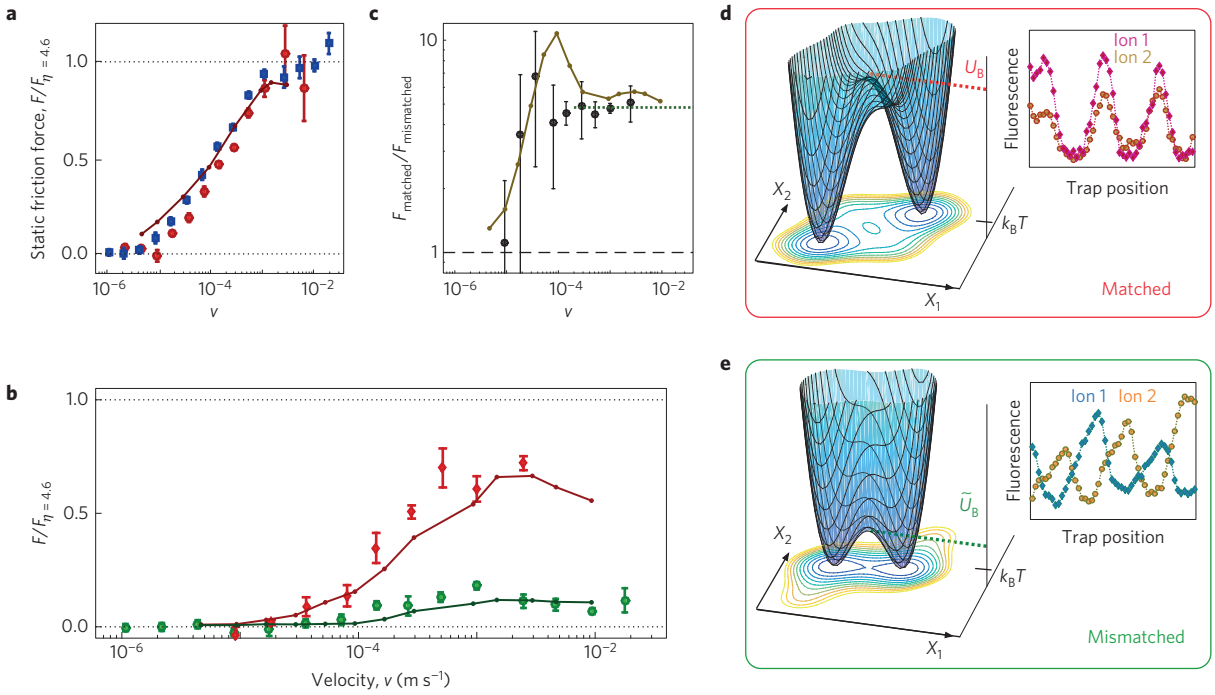

Figure 4 | Structural and thermal lubricity of two atoms. a–c, Velocity dependence of the friction force for two ions, for $\eta = 4.6$. **a**, In the matched case (red circles), where the ion spacing is an integer multiple of the lattice period a, for $k_BT/U_I = 0.055(10)$ the data agree with one ion at approximately the same temperature (blue squares), and reach a maximal value near $F_{\eta=4.6}$. Langevin simulations (solid lines) are in good agreement with data for $\eta = 4.6$, $k_BT/U_I = 0.05$. **b**, In the matched case (red diamonds) for a temperature of $k_BT/U_I = 0.15(2)$, the maximal friction is $\sim 0.7F_{\eta=4.6}$. By comparison, the friction for the mismatched case (green circles), where the two ions at their unperturbed position experience opposite forces by the optical lattice, at the same temperature of $k_BT/U_I = 0.15(3)$, reaches a maximum of $\sim 0.15F_{\eta=4.6}$. Finite-temperature Langevin simulations (solid lines) are in good agreement with data for $\eta = 4.6$, $k_BT/U_I = 0.15$. **c**, The ratio of friction forces in the matched and mismatched cases (black circles, 3-point running average) is unity in the low-velocity thermal drift regime, and constant in the high-velocity friction plateau regime, where its value ~ 4.8 is mostly due to structural lubricity, in good agreement with Langevin simulations (solid gold line). Although barely visible in the data, the peak in the simulations is due to structurally induced thermolubricity: a window of velocities for which the structural friction reduction is enhanced by thermal activation over a reduced energy barrier $\widetilde{U}_B$. **d**,**e**, Energy potential landscape for two interacting atoms. In the mismatched case (**e**), the energy barrier $\widetilde{U}_B$ between the wells is reduced by a factor of ~ 3.7 and the ions pass the barrier one at a time (inset), compared to the matched case U_B (**d**) where the ions pass the barrier simultaneously (inset). At fixed T for a single ion in the friction plateau regime, this barrier reduction $\widetilde{U}_B/U_B$ would lead to a thermal friction reduction of ~ 1.4, as can be inferred from the green data in Fig. 3. The expected total reduction of $3.7 \times 1.4 = 5.2$ is in good agreement with the observed reduction of ~ 4.8. Error bars are statistical and represent one standard deviation.

Received 7 May 2015; accepted 4 August 2015;
published online 14 September 2015

References

1. Urbakh, M., Klafter, J., Gourdon, D. & Israelachvili, J. The nonlinear nature of friction. *Nature* **430,** 525–528 (2004).
2. Vanossi, A., Manini, N., Urbakh, M., Zapperi, S. & Tosatti, E. Colloquium: Modeling friction: From nanoscale to mesoscale. *Rev. Mod. Phys.* **85,** 529–552 (2013).
3. Krylov, S. Y. & Frenken, J. W. M. The physics of atomic-scale friction: Basic considerations and open questions. *Phys. Status Solidi* **251,** 711–736 (2014).
4. Mate, C., McClelland, G., Erlandsson, R. & Chiang, S. Atomic-scale friction of a tungsten tip on a graphite surface. *Phys. Rev. Lett.* **59,** 1942–1945 (1987).
5. Dienwiebel, M. *et al.* Superlubricity of graphite. *Phys. Rev. Lett.* **92,** 126101 (2004).
6. Socoliuc, A., Bennewitz, R., Gnecco, E. & Meyer, E. Transition from stick–slip to continuous sliding in atomic friction: Entering a new regime of ultralow friction. *Phys. Rev. Lett.* **92,** 134301 (2004).
7. Gnecco, E. *et al.* Velocity dependence of atomic friction. *Phys. Rev. Lett.* **84,** 1172–1175 (2000).
8. Riedo, E., Gnecco, E., Bennewitz, R., Meyer, E. & Brune, H. Interaction potential and hopping dynamics governing sliding friction. *Phys. Rev. Lett.* **91,** 084502 (2003).
9. Liu, X.-Z. *et al.* Dynamics of atomic stick–slip friction examined with atomic force microscopy and atomistic simulations at overlapping speeds. *Phys. Rev. Lett.* **114,** 146102 (2015).
10. Li, Q., Dong, Y., Perez, D., Martini, A. & Carpick, R. W. Speed dependence of atomic stick–slip friction in optimally matched experiments and molecular dynamics simulations. *Phys. Rev. Lett.* **106,** 126101 (2011).
11. Zhao, X., Phillpot, S., Sawyer, W., Sinnott, S. & Perry, S. Transition from thermal to athermal friction under cryogenic conditions. *Phys. Rev. Lett.* **102,** 186102 (2009).
12. Jansen, L., Hölscher, H., Fuchs, H. & Schirmeisen, A. Temperature dependence of atomic-scale stick–slip friction. *Phys. Rev. Lett.* **104,** 256101 (2010).
13. Barel, I., Urbakh, M., Jansen, L. & Schirmeisen, A. Unexpected temperature and velocity dependencies of atomic-scale stick–slip friction. *Phys. Rev. B* **84,** 115417 (2011).
14. Medyanik, S., Liu, W., Sung, I.-H. & Carpick, R. Predictions and observations of multiple slip modes in atomic-scale friction. *Phys. Rev. Lett.* **97,** 136106 (2006).
15. Bylinskii, A., Gangloff, D. & Vuletic, V. Tuning friction atom-by-atom in an ion-crystal simulator. *Science* **348,** 1115–1118 (2015).
16. Karpa, L., Bylinskii, A., Gangloff, D., Cetina, M. & Vuletić, V. Suppression of ion transport due to long-lived subwavelength localization by an optical lattice. *Phys. Rev. Lett.* **111,** 163002 (2013).
17. Braun, O. M. & Kivshar, Y. S. *The Frenkel–Kontorova Model: Concepts, Methods, and Applications* (Springer, 2004).
18. Meyer, E. & Gnecco, E. Superlubricity on the nanometer scale. *Friction* **2,** 106–113 (2014).
19. Bohlein, T., Mikhael, J. & Bechinger, C. Observation of kinks and antikinks in colloidal monolayers driven across ordered surfaces. *Nature Mater.* **11,** 126–130 (2012).
20. Jagla, E. A. Velocity weakening and possibility of aftershocks in nanoscale friction experiments. *Phys. Rev. B* **86,** 155408 (2012).

21. Jinesh, K., Krylov, S., Valk, H., Dienwiebel, M. & Frenken, J. Thermolubricity in atomic-scale friction. *Phys. Rev. B* **78,** 155440 (2008).
22. Müser, M. Velocity dependence of kinetic friction in the Prandtl–Tomlinson model. *Phys. Rev. B* **16,** 1–15 (2011).
23. Dong, Y., Vadakkepatt, A. & Martini, A. Analytical models for atomic friction. *Tribol. Lett.* **44,** 367–386 (2011).
24. Sang, Y., Dubé, M. & Grant, M. Thermal effects on atomic friction. *Phys. Rev. Lett.* **87,** 174301 (2001).
25. Igarashi, M., Natori, A. & Nakamura, J. Size effects in friction of multiatomic sliding contacts. *Phys. Rev. B* **78,** 165427 (2008).
26. Benassi, A., Vanossi, A. & Tosatti, E. Nanofriction in cold ion traps. *Nature Commun.* **2,** 236 (2011).
27. Cetina, M. *et al.* One-dimensional array of ion chains coupled to an optical cavity. *New J. Phys.* **15,** 053001 (2013).
28. Pruttivarasin, T., Ramm, M., Talukdar, I., Kreuter, A. & Häffner, H. Trapped ions in optical lattices for probing oscillator chain models. *New J. Phys.* **13,** 075012 (2011).
29. Mandelli, D., Vanossi, A. & Tosatti, E. Stick–slip nanofriction in trapped cold ion chains. *Phys. Rev. B* **87,** 195418 (2013).
30. Enderlein, M., Huber, T., Schneider, C. & Schaetz, T. Single ions trapped in a one-dimensional optical lattice. *Phys. Rev. Lett.* **109,** 233004 (2012).
31. Linnet, R. B., Leroux, I. D., Marciante, M., Dantan, A. & Drewsen, M. Pinning an ion with an intracavity optical lattice. *Phys. Rev. Lett.* **109,** 233005 (2012).

Acknowledgements

We acknowledge support from the NSF-funded Center for Ultracold Atoms. D.G. and A.B. acknowledge funding from NSERC.

Author contributions

D.G., A.B. and V.V. designed the experiments. D.G., A.B. and I.C. collected and analysed data. All authors discussed the results and contributed to the manuscript preparation.

Additional information

Supplementary information is available in the online version of the paper. Reprints and permissions information is available online at www.nature.com/reprints. Correspondence and requests for materials should be addressed to V.V.

Competing financial interests

The authors declare no competing financial interests.